1987

NASA/ASEE SUMMER FACULTY RESEARCH FELLOWSHIP PROGRAM

MARSHALL SPACE FLIGHT CENTER
THE UNIVERSITY OF ALABAMA IN HUNTSVILLE

ATOMIC OXYGEN EFFECTS ON METALS

Prepared by:	Albert T. Fromhold, Ph.D.
Academic Rank:	Professor
University and Department:	Auburn University Department of Physics
NASA/MSFC: Laboratory: Division: Branch:	 Materials and Processes Engineering Physics Physical Sciences
MSFC Colleague:	Roger C. Linton
Date:	August 7, 1987
Contract No.:	The University of Alabama in Huntsville NGT-01-008-021

ATOMIC OXYGEN EFFECTS ON METALS

by

Albert T. Fromhold
Professor of Physics
Auburn University, AL 36849

ABSTRACT

The present work addresses the effect of specimen geometry on the attack of metals by atomic oxygen. This is done by extending the coupled-currents approach in metal oxidation to spherical and cylindrical geometries. Kinetic laws are derived for the rates of oxidation of samples having these geometries. It is found that the burn-up time for spherical particles of a given diameter can be as much as a factor of 3 shorter than the time required to completely oxidize a planar sample of the same thickness.

ACKNOWLEDGEMENTS

The author greatly appreciates the friendly hospitality extended to him by the personnel of the Materials and Processes Laboratory of Marshall Space Flight Center during his visit with them. He is grateful for the aid provided for him in the laboratory by his colleague, Roger C. Linton. He especially appreciates the help of John M. Reynolds in using the automated ellipsometer and Robert F. DeHaye in using the microprofiler. Several discussions with Ralph Carruth and Bruce Glick proved to be very helpful in setting up a program for continuation of the atomic oxygen studies. Finally, Dr. Gerald R. Karr, the UAH NASA/ASEE Summer Faculty Fellowship Program Director, and Mrs. Ernestine Cothran, Program Co-Director at MSFC, are to be highly commended for the outstanding seminars and activities which they carefully organized and subsequently supervised with such great flair.

INTRODUCTION

The failure of metal structures often occurs at cracks, corners, and crevices preferentially to planar surfaces. The present work addresses these geometric effects of the attack of atomic oxygen on metal surfaces.

OBJECTIVES

The objective of this work was to extend the coupled-currents approach for the oxidation of planar material surfaces to non-planar surfaces, specifically, surfaces having spherical and cylindrical symmetry.

CONCLUSIONS AND RECOMMENDATIONS

1. The burn-up rate can be significantly increased for non-planar geometries relative to planar geometries.

2. The theoretical development should be extended to include stress effects.

I. Concept of Steady-State Oxide Growth for Non-Planar Geometries

The focal point of this presentation is the effect of material sample geometry on the rate of oxidation. Because the oxidation rate is dependent upon the atom or ion current to the location where metal oxidation is occurring, it is necessary to evaluate the effects of sample geometry upon such currents. Frequently oxide formation occurs under fixed experimental conditions of ambient temperature and oxygen pressure, and in such situations the currents in the system are usually nearly steady-state.

The steady-state is a condition in which no change in the local value of the current takes place with time. Though thermodynamic equilibrium is a special case of the steady-state, the current then being uniformly zero, in general the steady-state differs from equilibrium.

To elaborate, current flows in response to driving forces, so currents are to be expected so long as the net driving force differs from zero. Currents may lead to a change in one or more components of the local driving force, in which case the net driving force may approach zero in time. Then the net current will approach zero in time, and a state of equilibrium is thereby attained. This evolution of the system can be expected for many, but not all, situations. A specific counter example is that of an externally-applied driving force and a closed-loop circuit around which the current can be sustained practically indefinitely, so the equilibrium state is not approached with time. In fact, there will be initial transients when the current is established, and it is the steady-state which is approached with time. Thus for some systems the long-time asymptotic limit on a laboratory time scale can be the steady-state, in contrast to equilibrium.

In the steady-state limit, the actual values of the local currents will depend directly upon the local values of the conductivity, as well as upon the local driving forces. The critical distinction between the steady-state and equilibrium, however, is in actuality one of net local driving force rather than actual value of the local current, even though in practice it may well be the measurable current that is used as the threshold criterion for equilibrium. Theoretically the values of the net local driving force must be zero everywhere in the system at equilibrium, and this naturally leads to the condition of zero current everywhere in the system, regardless of the value of the local conductivity.

The space-dependence of the current is likewise pertinent. For non-steady-state situations, the current can certainly vary locally with position. In the steady- state, however, the situation is not quite so intuitively clear. The local driving force or the local conductivity may vary with position initially, but the local driving force may adjust to compensate for the spatial variation of the conductivity. Care must be taken in the analysis of such cases. The critical aspect of the problem is that the spatial variation of the

current in the limit of the steady-state must be such that neither electric charge nor diffusing species concentrations build up or deplete anywhere within the system as the flow is maintained. This requires that the net current flowing into any region of space be equal to the net current flowing out of that region of space. Thus there must be no time-dependence of the local concentration of the mobile species. In vector terminology, the divergence of the current J in question must be zero,

$$(1)\quad -\partial C/\partial t = \nabla \cdot J = 0 \ ,$$

where C is the local mobile species concentration at time t. This condition will be shown to lead to the conclusion that even in the steady-state, the current can vary locally with position, depending on the geometry in question. Our attention is directed entirely to cases of thermal oxidation for which Eq. (1) represents a reasonably good approximation.

II. Ionic Current and Oxide Growth Rate

If the steady-state ionic current density J_i can be evaluated for the geometry in question, then the value of that current at the location where the chemical reaction of metal oxidation is occurring (usually one of the oxide interfaces) will enable a determination of the oxidation rate. Specifically, the ionic particle current density J_i at the reaction interface leads to an increase in the oxide film thickness L at that interface. The local oxide thickness formation rate at that location can be written as

$$(2)\quad \frac{dL}{dt} = R_i J_i \ ,$$

where R_i is the volume of oxide formed per transported particle of ionic species labeled i. The volume V_{oxide} of oxide being formed because of this oxide thickness increase is given by the product of the thickness increase with the area, summed over the reaction zone where oxide film formation is occurring. Assuming this to be either the interface between the sample and the oxide (designated the *metal- oxide interface*) or else the interface between the oxide and the oxygen being utilized for the reaction (designated the *oxide-oxygen interface*), then the oxide volume formation rate is given by

$$(3)\quad \frac{dV_{oxide}}{dt} = R_i \int_{\substack{Reaction \\ Interface}} J_i \cdot dA \ .$$

Note that the surface integral involves the vector dot product between the current density vector J_i and the differential area vector dA on the reaction interface. The current density vector is parallel to the motion of the species, and the differential area vector is locally perpendicular to the surface area where the current density vector is being evaluated. The effect of taking the vector dot product is to obtain the product of the current density flow perpendicular to the surface area with that surface area in order to obtain the total particle flow through the surface.

III. Sample Geometry

A. Domain of Application

Since the oxidation rate of materials is dependent upon the ionic currents through the protective oxide covering the material, it is necessary to evaluate the effects of sample geometry upon such currents. Our attention is now directed to the spatial variation of the steady-state current for cases of spherical and cylindrical symmetry. Spherical symmetry should well characterize the oxidation of spherical particles and should yield an approach to the oxidation within spherical cavities in materials. Cylindrical symmetry should well represent the oxidation of wires, and should model reasonably well the oxidation of edges formed by intersection of two planar surfaces.

B. Spherically-Symmetric Case

Consider a uniform radial flow of current density J_s of species s between two concentric metal spheres having radii a and b, with $a < b$, which can be called the inner and outer electrodes. If none of the species concentrations C_s change at any vector position r with time t, the condition necessary for the steady-state, then the total current I_s of species s given by

$$(4) \quad I_s = \int_{\substack{\text{Symmetry} \\ \text{Sphere of} \\ \text{Radius r}}} J_s(r)\, dA = J_s(r)[4\pi r^2]$$

must be the same when evaluated over any imagined sphere concentric with the spherical electrodes, assuming $a < r < b$. The spherical symmetry insures that J_s is independent of the position of the area element dA on the sphere of radius r. That is, there is no preferred radial direction of flow in a spherically-symmetric situation such as this, so the current density is uniform over the surfaces of symmetry consistent with the physical system. This allows the ready evaluation of the surface integral in Eq. (4).

The fact that the total current I_s is independent of the radius r of the chosen sphere in Eq. (4) means that for a spherical shell volume element bounded by two such spherical surfaces, the current out of the volume element will equal the current into the volume element. Thus there will be no build-up or depletion of the concentration of the species within the volume element, as required by the steady-state condition.

The conclusion to be derived from Eq. (4) is that the steady-state radial current density for the case of spherical symmetry varies inversely with the square of the distance r,

$$(5) \quad J_s(r) \propto 1/r^2 \ .$$

C. Cylindrically-Symmetric Case

If the two metal electrodes are concentric cylinders instead of being concentric spheres, then the current will likewise be radial if the medium between the two electrodes is uniform. Equation (4) is then replaced by

$$(6)\quad I_s = \int_{\substack{\text{Symmetry}\\ \text{Cylinder of}\\ \text{Radius r}}} J_s(r)\, dA = J_s(r)[2\pi rh] \ ,$$

where h is the length of the concentric cylindrical electrodes having radii a and b ($a < r < b$). The steady-state in this case likewise requires that I_s be independent of r, where in this case r is the radius of any imagined cylinder of symmetry with the electrodes ($a < r < b$). The symbol dA in this case is the area element on the cylinder of radius r. The uniformity of the current density J_s , which because of the electrode symmetry is in the radial direction and has the same value at any point on a given symmetry cylinder, leads to the ready evaluation of the surface integral as shown in Eq. (6). There is no need to consider the flat ends of the imagined cylinder in Eq. (6), since there would be no contribution to I_s from a surface integral over those regions because there is no current perpendicular to the flat ends of the cylinder. The separation distance h between the ends of the imagined cylinder does enter into Eq. (6) because the surface area of the curved portion of the cylindrical surface through which the current flows depends upon the length of the cylinder.

The independence of the total current I_s on radius r of the chosen cylinder in Eq. (6) means that for a cylindrical shell volume element bounded by two such cylindrical surfaces, the current out of the volume element will be equal to the current into the volume element. Thus there will be no build-up or depletion of the concentration of the species within the volume element, as required by the steady-state condition.

The conclusion to be derived from Eq. (6) is that the steady-state radial current density for the case of cylindrical symmetry varies inversely with the distance r,

$$(7)\quad J_s(r) \propto 1/r \ .$$

D. Planar-Symmetric Case

For completeness, let us carry out the above analysis for two metal electrodes which are symmetrically-located parallel planes separated by some distance L. The current will be perpendicular to the electrodes if the medium between the two electrodes is uniform. Equation (4) is then replaced by

$$(8)\quad I_s = \int_{\substack{\text{Symmetry}\\ \text{Rectangle at}\\ \text{Position x}}} J_s(x)\, dA = J_s(x)\, A \ ,$$

where A is the total area of the rectangle. The steady-state in this case also requires that I_s be independent of x, where x is the distance to the rectangle, as measured perpendicularly from one of the electrodes.

The symbol dA in this case is the area element on the rectangle. The uniformity of the current density J_s , which because of the electrode symmetry is in the perpendicular direction and has the same value at any point on a given symmetry rectangle, leads to the easy

evaluation of the surface integral as shown in Eq. (8). There is no dependence of I_s on the position x of the rectangle, as noted from Eq. (6). In addition, there is no dependence on the electrode separation distance L.

The independence of the total current I_s on position x of the rectangle in Eq. (8) means that for a parallelepiped volume element bounded by two such rectangular surfaces, the current out of the volume element will be equal to the current into the volume element. There would be no current through the four ends of the parallelepiped because the current density is parallel to those planar ends. Thus there will be no build-up or depletion of the concentration of the species within the volume element, as required by the steady-state condition.

The conclusion to be derived from Eq. (8) is that the steady-state current density for the case of planar symmetry does not vary with the position x in the medium,

(9) $J_s \propto$ *Constant, independent of poxition* x .

To summarize, the steady-state current density is independent of position for planar geometry, it decreases inversely as the radial position r for cylindrical symmetry, and it decreases inversely as the square of the radial distance for spherical symmetry.

E. More Formal Treatment

We can treat the problems of spherical, cylindrical, and planar symmetry more formally by introducing the corresponding vector forms for the divergence operator in the appropriate orthogonal coordinate systems.

The divergence operator in the spherical polar coordinate system is given by

$$(10) \quad \nabla\cdot\mathbf{J} = \frac{1}{r^2 \sin\theta}\left[\sin\theta\,\frac{\partial}{\partial r}(r^2 J_r) + r\,\frac{\partial}{\partial\theta}(\sin\theta\, J_\theta) + r\,\frac{\partial}{\partial\phi}(J_\phi)\right]$$

where the vector

$$(11) \quad \mathbf{J} = \hat{\mathbf{r}}\, J_r + \hat{\boldsymbol{\theta}}\, J_\theta + \hat{\boldsymbol{\phi}}\, J_\phi$$

in spherical polar coordinates r, θ, and ϕ has the components J_r, J_θ, and J_ϕ, with $\hat{\mathbf{r}}$, $\hat{\boldsymbol{\theta}}$, and $\hat{\boldsymbol{\phi}}$ being the unit vectors in that coordinate system. Because in our application, **J** represents the current which is entirely radial and moreover is a function of r only, $J_r = J_r(r)$, $J_\theta = 0$, and $J_\phi = 0$. Equation (10) for the divergence reduces in this case to

$$(12) \quad \nabla\cdot\mathbf{J} = \frac{1}{r^2}\,\frac{\partial}{\partial r}(r^2 J_r) \ .$$

Applying the steady-state condition in the form of Eq. (1) then leads to

$$(13) \quad \frac{\partial}{\partial r}\left[r^2 J_r(r)\right] = 0 \ ,$$

which integrates to yield

$$(14) \quad r^2 J_r(r) = \mathcal{K}_{sph}$$

with $\mathcal{K}_{sph}$ being the constant of integration. Thus we obtain $J \propto 1/r^2$ for this case, in accordance with Eq. (5) previously deduced. By comparing this result with Eq. (4) we see that $\mathcal{K}_{sph}=I_s/4\pi$.

The divergence operator in the cylindrical polar coordinates is given by

$$(15) \quad \nabla\cdot J = \frac{1}{r}\frac{\partial}{\partial r}(r\, J_r) + \frac{1}{r}\frac{\partial}{\partial \theta}(J_\theta) + \frac{\partial}{\partial z}(J_z) \ ,$$

where the vector

$$(16) \quad J = \hat{r}\, J_r + \hat{\theta}\, J_\theta + \hat{z}\, J_z$$

in cylindrical polar coordinates r, θ, and z has the components J_r , J_θ , and J_z , with $\hat{r}$, $\hat{\theta}$, and $\hat{z}$ being the unit vectors in that coordinate system. However, in cylindrical symmetry cases, the current density vector is radial. Therefore, in cylindrical polar coordinates, the component J_r is the only non-zero component of the vector; the components J_θ and J_z are zero. Moreover, J_r is a function of r only. Thus we can write

$$(17) \quad \nabla\cdot J = \frac{1}{r}\frac{\partial}{\partial r}(r\, J_r).$$

Applying the steady-state condition in the form of Eq. (1) then leads to

$$(18) \quad \frac{\partial}{\partial r}\left[\, r\, J_r(r) \,\right] = 0 \ ,$$

which integrates to give

$$(19) \quad r\, J_r(r) = \mathcal{K}_{cyl} \ ,$$

with $\mathcal{K}_{cyl}$ being the constant of integration. Thus we obtain $J \propto 1/r$ for this case, in accordance with Eq. (7) previously deduced. By comparing this result with Eq. (6) we see that $\mathcal{K}_{cyl}=I_s/2\pi h$.

For completeness, let us also carry out the above analysis for planar symmetry, where any variation is considered to occur in the $\hat{x}$-direction, with the system being entirely uniform in the $\hat{y}$ and $\hat{z}$-directions. The divergence operator in rectangular cartesian coordinates is given by

$$(20) \quad \nabla\cdot J = \frac{\partial J_x}{\partial x} + \frac{\partial J_y}{\partial y} + \frac{\partial J_z}{\partial z}$$

where the vector

$$(21) \quad J = \hat{x}\, J_x + \hat{y}\, J_y + \hat{z}\, J_z$$

in rectangular cartesian coordinates x, y, and z has the components J_x , J_y , and J_z , with $\hat{x}$, $\hat{y}$, and $\hat{z}$ being the unit vectors in that coordinate system. However, in the presently-considered case, the current density vector is in the $\hat{x}$ direction and moreover is at most a

function of the x-coordinate. Thus

$$(22) \quad \nabla \cdot J = \frac{\partial J_x(x)}{\partial x} \ .$$

Applying the steady-state condition in the form of Eq. (1) then leads to

$$(23) \quad \frac{\partial J_x(x)}{\partial x} = 0 \ .$$

which integrates to yield

$$(24) \quad J_x(x) = \aleph_{plane} \ ,$$

with $\aleph_{plane}$ being the constant of integration. Thus we obtain J_x independent of x for this case, in accordance with Eq. (9) previously deduced.

In the following section we show how to proceed in obtaining the values of the total current. This is tantamount to evaluating the integration constants obtained above.

IV. Driving Forces and Currents

The general vector relation for the current density J_s for species s in terms of the electrochemical potential $\tilde{u}_s$ for species s is determined by the vector gradient,

$$(25) \quad J_s \propto - C_s \nabla \tilde{u}_s \ ,$$

where C_s is the concentration of species s. The form for the gradient operator ∇ is specific to the symmetry of the physical problem to be treated. It can be expressed, for example, in rectangular, spherical, and cylindrical coordinates, or in a more general form which applies to any orthogonal curvilinear coordinate system. In spherical polar coordinates,

$$(26) \quad \nabla \tilde{u}_s = \hat{r} \frac{\partial \tilde{u}_s}{\partial r} + \hat{\theta} \frac{1}{r} \frac{\partial \tilde{u}_s}{\partial \theta} + \hat{\phi} \frac{1}{r \sin \theta} \frac{\partial \tilde{u}_s}{\partial \phi} \ ,$$

while in cylindrical polar coordinates,

$$(27) \quad \nabla \tilde{u}_s = \hat{r} \frac{\partial \tilde{u}_s}{\partial r} + \hat{\theta} \frac{1}{r} \frac{\partial \tilde{u}_s}{\partial \theta} + \hat{z} \frac{\partial \tilde{u}_s}{\partial z} \ .$$

Denoting the proportionality factor for Eq. (25) by $\mathfrak{B}_s$, and using the standard form for the electrochemical potential,

$$(28) \quad \tilde{u}_s = u_s^o + k_B T \ln C_s + q_s V \ ,$$

where u_s^o is the reference state value of the chemical potential u_s , k_B is Boltzmann's constant, T is the absolute temperature, q_s is the charge per particle of species s, and V is the electrostatic potential, Eq. (25) becomes

$$(29) \quad J_s = - \mathfrak{B}_s C_s \nabla \tilde{u}_s = - k_B T \mathfrak{B}_s \nabla C_s + q_s \mathfrak{B}_s E C_s \ ,$$

where **E** is the electric field given by

(30) $\mathbf{E} = - \nabla V$.

Comparison with the usual linear diffusion equation

(31) $J_s = - D_s \nabla C_s + \mu_s \mathbf{E} C_s$,

shows term-by-term agreement, with the diffusion coefficient being given by

(32) $D_s = k_B T \mathcal{B}_s$

and the mobility being given by

(33) $\mu_s = q_s \mathcal{B}_s$.

The ratio of the two coefficients gives the Einstein relation

(34) $\mu_s / D_s = q_s / k_B T$.

The electric field is of course zero in the above equations if the diffusing species giving rise to the oxidation process are uncharged. With this choice, the equations in our development for the rate of oxidation yield also the growth rate for non-planar geometries for the diffusion of uncharged particles. In this limit the results can be compared to those deduced by Wilson and Marcus[1]. Generally the diffusing species are charged, however, in which case the full treatment is required.

V. Electric Fields

A. Generals Relations and Zero-Space-Charge Limit

For charged particle diffusion, the driving force of the electric field is as important as the concentration gradient, both being included as part of the gradient in the electrochemical potential[2]. For cases of high symmetry, Gauss' law provides the easiest approach to finding the value and position-dependence of the field. A closed imaginary surface having the symmetry of the physical problem is used for carrying out a surface integral of the electric field,

(35) $$\int_{\substack{\text{Imaginary} \\ \text{Surface}}} \varepsilon \, \mathbf{E} \cdot d\mathbf{A} = Q$$

where Q is the net charge within the closed surface that is chosen for the integration. The parameter ε is the electric permittivity of the medium.

The relationship between the electric field **E** and the electric potential difference V_{ab} between points b and a is given by the line integral

(36) $V_{ab} = - \int_a^b \mathbf{E} \cdot d\mathbf{r}$,

which is in accord with Eq. (30). The magnitude of the potential difference between two electrodes is usually called the applied voltage.

There can be space-charge contributions to the field as well as surface-charge contributions, but for diffusing defect densities below $10^{16}/cm^3$ for example, the space-charge contributions may be neglected for oxide thicknesses below 1000 Å or so.[3] Because the space charge is a complexity in itself, in the present development we choose to neglect it. The present development is therefore restricted to the zero space-charge limit, so that the electric field is due to surface charge only. In the case of planar oxides, the zero space-charge limit leads to electric fields which are independent of position x within the oxide, and for this reason it has been designated[2] the "*homogeneous-field approximation*". At the moment, we restrict our consideration to the zero space-charge limit in order to focus more intensely on the purely geometric effects which is the subject of this presentation.

B. Spherical Geometry

Consider specifically the spherical geometry case with concentric spherical electrodes of radius a and b, with $a < b$. The electric field does not require the existence of electrodes, but it is helpful to imagine that they are present. Radial symmetry and zero space charge in the uniform medium leads to a ready evaluation of Gauss' law for this case,

$$(37) \quad \varepsilon E_r 4\pi r^2 = Q_a , \qquad (a < r < b)$$

where Q_a is the charge on the inner electrode a. The radial component of the field is the only nonzero component, as can be argued convincingly from the symmetry of the physical problem.

The corresponding electric potential difference evaluated at some arbitrary position r between the electrodes is given by

$$(38) \quad V(r) - V(a) = -\int_a^r E_r \, dr = \frac{Q_a}{4\pi\varepsilon}\left(\frac{1}{r} - \frac{1}{a}\right)$$

The total built-in electric potential across the oxide is given by this expression evaluated at $r = b$,

$$(39) \quad V_{built\text{-}in} = V(b) - V(a) = \frac{Q_a}{4\pi\varepsilon}\left(\frac{1}{b} - \frac{1}{a}\right) .$$

With no space charge, the charge Q_b at b is the negative of Q_a ,

$$(40) \quad Q_b = - Q_a .$$

The specific evaluation of $V_{built\text{-}in}$ will be carried out subsequently.

C. Cylindrical Geometry

Consider concentric cylindrical electrodes of radius a and b, with $a < b$. Gauss' law leads to

$$(41) \quad \varepsilon E_r 2\pi r h = Q_a \qquad (a < r < b)$$

where the total charge Q_a on electrode a is determined by the charge λ per unit length of that electrode,

(42) $Q_a = \lambda\, h$.

Conservation of charge and the absence of space charge allows writing

(43) $Q_b = - Q_a$.

As in the spherical geometry case, the radial component is the only nonzero component of the field.

The electric potential V(r) for this cylindrically-symmetric case is given by

(44) $V(r) - V(a) = - \int_a^r E_r\, dr = -(\lambda_a/2\pi\varepsilon)\ln(r/b)$.

The total built-in electric potential across the oxide is given by this expression evaluated at r = b,

(45) $V_{built\text{-}in} = V(b) - V(a) = -(\lambda/2\pi\varepsilon)\ln(b/a)$.

D. Planar Symmetry

For completeness, let us give the analogous results for planar geometry. For the metal-oxide interface at a and the oxide-oxygen interface at b, the oxide thickness is given by L=b-a. Planar symmetry and zero space charge leads to a ready evaluation of Gauss' law,

(46) $\varepsilon\, E_x\, A = Q_a$,

where $\tau = Q_a/A$ is the charge per unit area. The corresponding electric potential is given by

(47) $V(x) - V(a) = (\tau/\varepsilon)(x - a)$.

Evaluation of this expression at x = b gives the potential difference across the oxide.

E. More Formal Treatment

A more formal treatment can be based on Poisson's equation

(48) $-\nabla^2 V = \rho/\varepsilon$,

where ρ is the local volume charge density and ε is the electric permittivity of the oxide. For zero space charge, ρ=0. Employing $\mathbf{E} = -\nabla V$, this leads to

(49) $-\nabla^2 V = -\nabla \cdot \nabla V = \nabla \cdot \mathbf{E} = 0$.

In spherical polar coordinates this becomes

$$(50)\quad \frac{1}{r^2 \sin\theta}\left[\sin\theta\,\frac{\partial}{\partial r}(r^2 E_r) + r\,\frac{\partial}{\partial\theta}(\sin\theta\, E_\theta) + r\frac{\partial E_\phi}{\partial\phi}\right] = 0\ ,$$

while in cylindrical polar coordinates this relation is

$$(51)\quad \frac{1}{r}\frac{\partial}{\partial r}(r E_r) + \frac{1}{r}\frac{\partial E_\theta}{\partial\theta} + \frac{\partial E_z}{\partial z} = 0\ .$$

Due to the spherical and cylindrical symmetry assumed in the respective cases, only the radial component of the field is nonzero. Furthermore, $E_r = E_r(r)$ only, since, with the specified symmetries, there is no cause for variation of the field in the other directions. Thus we obtain in the spherically-symmetric case

$$(52)\quad \frac{\partial}{\partial r}(r^2 E_r) = 0\ ,$$

while for the cylindrically-symmetric case we obtain

$$(53)\quad \frac{\partial}{\partial r}(r E_r) = 0\ .$$

These expressions are readily integrated. Thus for spherical symmetry,

$$(54)\quad E_r \propto \frac{1}{r^2}\ ,$$

while for cylindrical symmetry,

$$(55)\quad E_r \propto \frac{1}{r}\ ,$$

in accordance with the above results obtained using Gauss' law. The planar case is just as simple, since for zero space charge,

$$(56)\quad \nabla\cdot\mathbf{E} = \frac{\partial E_x}{\partial x} + \frac{\partial E_y}{\partial y} + \frac{\partial E_z}{\partial z} = 0\ .$$

For symmetry over planes perpendicular to $\hat{x}$, we expect that E_y=0 and E_z=0, and that E_x will be independent of y and z. Thus

$$(57)\quad \frac{\partial E_x}{\partial x} = 0\ ,$$

and

$$(58)\quad E_x = \textit{Constant}\ .$$

The electrical potentials follow from a line integral of the electric field in the usual way, as already shown above.

VI. Coupled Currents for Spherical and Cylindrical Symmetries

A. Coupled-Currents Condition

Let us consider the interface between the material being oxidized (usually a metal) and the oxide layer to be located by the radius a. This is the metal-oxide interface. Then the opposite interface of the oxide, which is the oxide-oxygen interface in contact with the attacking oxygen phase, is considered to be located by the radius b. As the oxide film grows, both a and b change. In spherical,

cylindrical, and planar geometries, the oxide film thickness L is given by the difference between a and b, so a = a(t) and b = b(t).

The electrochemical potential difference between the metal-oxide and the oxide-oxygen interfaces provides the driving force for the currents, as outlined above. At any position in the oxide layer, the existing electric field will aid transport of the ionic or the electronic species, and oppose transport of the other. The currents can themselves lead to a net charge transport, which changes the field since Q_a will be modified. Careful analysis[2] has shown that the net charge transported through the oxide layer of thickness L over any time increment is generally much smaller than the charge transported by either the ions or the electrons individually. Were this not the case, the electric fields produced within the system would reach catastrophic values very quickly, with dielectric breakdown occurring. The fundamental point is that a monolayer of charged particles can produce an incredibly large electric field, so that the net charge setting up the surface-charge field requires only a tiny imbalance in positive and negative charge. The difference between the positive and negative charge transport during the building of a layer of oxide can represent at most only a tiny fraction of the total particles in that layer.

The coupled-currents condition

$$(59) \quad q_1 J_1 + q_2 J_2 = 0$$

represents a state of zero net charge transport, since the charge current $q_1 J_1$ of the ionic species (species 1) is nullified by the charge current $q_2 J_2$ of the electronic species (species 2). This presumes the specific situation where there is one dominant diffusing ionic species and one dominant diffusing electronic species, which is the simplest case for growth by charged particles.

The coupled currents condition has been used widely in the evaluation of planar oxide growth[2], but to date it has not been applied to the growth of non-planar oxides. For the spherical and the cylindrical symmetries, the currents $J_s(r)$ given by Eqs. (4) and (8) respectively, can be substituted into Eq. (59) above to obtain the following form for the coupled-currents condition,

$$(60) \quad q_1 I_1 + q_2 I_2 = 0 \ .$$

This is the most useful form for present purposes.

B. Differential Equation for the Current

The current density J_s of species s is given in general, by Eq. (29). The geometry in question determines the form of the gradient operator ∇ and the functional form of the electric field **E**. In both the spherical and the cylindrical geometries, C_s varies only radially, so that $C_s = C_s(r)$. The gradient operation in both geometries [see Eqs. (26) and (27)] then reduces to the especially simple form

$$(61) \quad \nabla C_s = \hat{\mathbf{r}}(dC_s/dr) \ ,$$

where $\hat{r}$ is the unit vector in the radial direction. In both geometries the electric field is radial, so that

$$(62) \quad \mathbf{E} = \hat{r}\, E_r \ .$$

Substituting these two relations into Eq. (29) yields the current

$$(63) \quad \mathbf{J}_s = \hat{r}\, J_s$$

which is totally radial, with J_s given by

$$(64) \quad J_s = - k_B T \, \mathscr{B}_s \frac{dC_s}{dr} + q_s \, \mathscr{B}_s \, E_r \, C_s \ .$$

VII. Solution of Problem for Spherical Symmetry

A. Concentration Profile and Steady-State Current

The electric field for spherical symmetry given by Eq. (37) can be substituted into Eq. (64) for the current, and in addition Eq. (4) can be used to replace the position-dependent current density J_s by the position-independent quantity I_s. Thus we obtain

$$(65) \quad \frac{I_s}{4\pi r^2} = - k_B T \, \mathscr{B}_s \frac{dC_s}{dr} + q_s \, \mathscr{B}_s \, C_s \frac{Q_a}{4\pi\varepsilon r^2} \ .$$

Rearranging this equation to separate variables yields the integral form

$$(66) \quad \int_{C_s(a)}^{C_s(r)} \frac{(4\pi\varepsilon k_B T \mathscr{B}_s) dC_s}{(q_s \mathscr{B}_s Q_a) C_s - \varepsilon I_s} = \int_a^r \frac{dr}{r^2} \ .$$

These integrals are readily evaluated to give the concentration profile,

$$(67) \quad C_s(r) = (\varepsilon I_s / q_s \mathscr{B}_s \, Q_a) + \left[C_s(a) - (\varepsilon I_s / q_s \mathscr{B}_s \, Q_a) \right] P_s(r) \ ,$$

where

$$(68) \quad P_s(r) = \exp\left[\alpha_s [(1/a) - (1/r)] \right] ,$$

with

$$(69) \quad \alpha_s = q_s Q_a / 4\pi\varepsilon k_B T \ .$$

The total particle current I_s for species s then follows by evaluating the concentration profile expression at r=b,

$$(70) \quad I_s = (q_s \, Q_a \, \mathscr{B}_s / \varepsilon) \left[\frac{C_s(b) - C_s(a) P_s(b)}{1 - P_s(b)} \right] \ .$$

Thus I_s is given in terms of Q_a and otherwise known parameters of the system for any species s.

The subsequent algebraic details are simplified by introducing the parameter Γ defined by

(71) $\Gamma = \exp\left[\alpha_o[(1/a)-(1/b)]\right]$,

where

(72) $\alpha_o = eQ_a/4\pi\varepsilon k_B T$,

with e representing the electronic charge magnitude. Expressing the charge q_s per particle of species s as

(73) $q_s = Z_s e$,

the quantity $P_s(b)$ appearing in Eq. (70) becomes

(74) $P_s(b) = \Gamma^{Z_s}$,

since

(75) $\alpha_s = Z_s \alpha_o$.

B. Built-in Potential

To determine Q_a , we now invoke the coupled currents condition. Substituting Eq. (70) for I_s (with s=1 and s=2) into Eq. (60) and utilizing Eqs. (73)-(74) yields

(76) $$\frac{Z_1^2 \mathfrak{R}_1 [C_1(a)\Gamma^{Z_1} - C_1(b)]}{\Gamma^{Z_1} - 1} + \frac{Z_2^2 \mathfrak{R}_2 [C_2(a)\Gamma^{Z_2} - C_2(b)]}{\Gamma^{Z_2} - 1} = 0 .$$

This represents an algebraic equation for Γ, and the solution yields the quantity Q_a because that is the only variable quantity in the definition of Γ, as can be noted from Eqs. (71) and (72). This in turn is sufficient to evaluate $V_{built\text{-}in}$ by means of Eq. (39). Thus

(77) $V_{built\text{-}in} = -(k_B T/e) \ln \Gamma$.

The details of solving the algebraic equation for Γ hinges upon the ratio Z_1/Z_2 , but this is a technical problem only. The important point is that the solution will yield a value for Γ which depends upon the fixed parameters of the system but which under normal circumstances will be independent of the values of the radii a and b. Thus Γ will not depend upon the thickness of the oxide, and hence the built-in potential $V_{built\text{-}in}$ will be fixed during growth of the oxide. This is a very important result for the kinetics of oxidation for the case of spherical geometry.

At this point it is worthwhile to find the explicit forms for the built-in potential for some specific situations. Consider first the ionic species to be monovalent cation interstitials, in which case $Z_1 = 1$, with the attendant electronic species being electrons, so $Z_2 = -1$. The solution of Eq. (76) is readily obtained,

(78) $\Gamma = [\mathfrak{R}_1 C_1(b) + \mathfrak{R}_2 C_2(a)] / [\mathfrak{R}_1 C_1(a) + \mathfrak{R}_2 C_2(b)]$, $\quad (Z_1=+1;\ Z_2=-1)$

and the built-in potential follows immediately from Eq. (77).

Since this result is independent of the radii a and b, it follows that it must also give the corresponding value for the built-in potential in the planar limit where L=(b-a) is small relative to a. [Refer to ch. 7, §3 in Ref. 2 for the planar treatment].

For the converse case of monovalent cation vacancies and electron holes, $Z_1 = -1$ and $Z_2 = +1$. The same form of equation results, but with Γ replaced by $1/\Gamma$. Thus the solution for Γ for this case is the reciprocal of the right-hand side of Eq. (78) above. The built-in potential will then have the same magnitude but will be of opposite sign.

Whenever the ionic species is divalent, the ratio Z_1/Z_2 will have the value -2. This case may involve cation interstitials ($Z_1=+2$) with electrons, or else cation vacancies ($Z_1=-2$) with electron holes. In either case a quadratic equation for Γ emerges, but this is readily solved by the quadratic formula. The value of Γ will be independent of the thickness of the oxide, so the built-in potential given by Eq. (77) will be independent of oxide thickness.

C. Ionic Current for Spherical Samples

The total ionic current I_1 is readily evaluated at this point, since the evaluation of Γ is sufficient to yield $P_s(b)$ from Eq. (74) above, and also sufficient to yield α_o and hence Q_a from Eqs. (71)-(72),

$$(79)\quad Q_a = (4\pi\varepsilon k_B T/e)\left(\frac{1}{a} - \frac{1}{b}\right)^{-1} \ln \Gamma \ .$$

Thus the charge on the metal changes with the radii a and b as the oxide grows. This technically is a violation of the coupled-currents condition, but it can be shown to provide only a minor perturbation on the final result.

Utilizing the above result for Q_a ,we obtain from Eq. (70) for I_1 the following expression for the total ionic current,

$$(80)\quad I_1 = 4\pi Z_1 \mathfrak{R}_1 k_B T \ln(\Gamma)\left(\frac{1}{a} - \frac{1}{b}\right)^{-1}\left[\frac{C_1(b) - C_1(a)\Gamma^{Z_1}}{1 - \Gamma^{Z_1}}\right].$$

Alternatively, the total current may be expressed in terms of the constant built-in potential,

$$(81)\quad I_1 = -4\pi q_1 \mathfrak{R}_1 \left(\frac{1}{a} - \frac{1}{b}\right)^{-1} V_{built\text{-}in} \times \left[\frac{C_1(b) - C_1(a)\exp[-Z_1 e V_{built\text{-}in}/k_B T]}{1 - \exp[-Z_1 e V_{built\text{-}in}/k_B T]}\right].$$

For the positive monovalent ionic species case, the evaluation of $V_{built\text{-}in}$ given by Eqs. (77)-(78) can be inserted directly into this expression to obtain an alternate form, if desired.

D. Oxide Growth and Particle Burnup Rate Laws for Spherical Samples

Because I_1 gives the total current flowing through any symmetry sphere, as defined in Eq. (4), and moreover is independent of the

radius of the sphere chosen, it represents the value of the integral appearing in Eq. (3) for the volume rate of oxide formation. Thus we can write

$$(82)\quad \frac{dV_{oxide}}{dt} = R_1 I_1 ,$$

where I_1 is the total ionic current as evaluated above. Since I_1 is given in terms of the time-dependent radii a and b, it is necessary to relate these quantities to V_{oxide} before the growth law can be evaluated.

Let us next define the volume expansion parameter σ,

$$(83)\quad \sigma = \frac{\text{Volume of oxide formed}}{\text{Volume of metal used in oxide formation}}$$

Since the volume of metal which has been utilized at any time t is given by

$$(84)\quad V_{metal} = \frac{4}{3}\pi a_o^3 - \frac{4}{3}\pi a^3 ,$$

where a_o is the radius of the metal sphere at t=0, the corresponding volume of oxide which has been formed is given by

$$(85)\quad V_{oxide} = \left(\frac{4}{3}\pi b^3 - \frac{4}{3}\pi a^3\right) - \left(\frac{4}{3}\pi b_o^3 - \frac{4}{3}\pi a_o^3\right) ,$$

where b_o locates the oxide-oxygen interface at t=0. If no initial oxide is present, then $b_o = a_o$, and the above expression simplifies accordingly. The volume expansion parameter thus can be written as

$$(86)\quad \sigma = \frac{(b^3 - b_o^3) + (a_o^3 - a^3)}{a_o^3 - a^3} = 1 + [(b^3 - b_o^3)/(a_o^3 - a^3)] ,$$

which provides the following relation between b and a,

$$(87)\quad b = \left[b_o^3 + (\sigma - 1)(a_o^3 - a^3)\right]^{1/3} .$$

Whenever the volume of oxide exceeds the volume of metal consumed in forming the oxide, σ exceeds unity. For a negligible expansion in volume upon oxide formation, σ would be unity and b would maintain its t=0 value b_o . Since in general

$$(88)\quad V_{oxide} = \sigma V_{metal} ,$$

we obtain from Eq. (84),

$$(89)\quad \frac{dV_{oxide}}{dt} = \sigma \frac{dV_{metal}}{dt} = -4\pi\sigma a^2 \frac{da}{dt}$$

Setting this equal to $R_1 I_1$ in accordance with Eq. (82) above gives

$$(90)\quad -\sigma a^2 \frac{da}{dt}\left(\frac{1}{a} - \frac{1}{b}\right) = \Omega ,$$

where Ω is the constant quantity

$$(91)\quad \Omega = - R_1 \mu_1 V_{built\text{-}in}\left[\frac{C_1(b) - C_1(a)\exp[-Z_1 eV_{built\text{-}in}/k_B T]}{1 - \exp[-Z_1 eV_{built\text{-}in}/k_B T]}\right] ,$$

with μ_1 being the ionic mobility defined by Eq. (33). Next we can utilize Eq. (87) for b in terms of a, and integrate the above differential equation from t = 0 to arbitrary time t,

$$(92) \quad \frac{1}{2}\,\sigma\,[a_o^2 - a^2] + \sigma\,\mathcal{I}_1(a) = \Omega\,t\ ,$$

where

$$(93) \quad \mathcal{I}_1(a) = \int_{a_o}^{a} \frac{a^2\,da}{\left(b_o^3 + (\sigma - 1)(a_o^3 - a^3)\right)^{1/3}}\ .$$

The integral $\mathcal{I}_1(a)$ is easily evaluated,

$$(94) \quad \mathcal{I}_1(a) = -\frac{1}{2(\sigma - 1)}\left[\left(b_o^3 + (\sigma - 1)(a_o^3 - a^3)\right)^{2/3} - b_o^2\right]$$

We note in passing that $\mathcal{I}_1(a)$ can likewise be written in terms of b,

$$(95) \quad \mathcal{I}_1 = -\frac{1}{2(\sigma - 1)}\left[b^2 - b_o^2\right].$$

Combining the integrated form for $\mathcal{I}_1(a)$ with Eq. (92) yields the rate law for the time-rate of change of the radius a(t) of the metal particle.

Next let us deduce the corresponding rate law for the variation of the outer radius b with time. From Eq. (87) which relates b to a we obtain by differentiation

$$(96) \quad a^2\,da = -(\sigma - 1)^{-1}\,b^2\,db\ .$$

Substituting this relation into Eq. (90) yields

$$(97) \quad \left(\frac{\sigma}{\sigma - 1}\right)\left[\frac{b^2}{a}\frac{db}{dt} - b\frac{db}{dt}\right] = \Omega\ .$$

Integrating this equation from t=0 to arbitrary time t yields the rate law for the outer radius b(t),

$$(98) \quad \left(\frac{\sigma}{\sigma - 1}\right)\left[\mathcal{I}_2(b) - \frac{1}{2}\,[b^2 - b_o^2]\right] = \Omega\,t\ ,$$

where, employing Eq. (87),

$$(99) \quad \mathcal{I}_2(b) = \int_{b_o}^{b} \frac{b^2\,db}{\left(a_o^3 - (\sigma - 1)^{-1}[b^3 - b_o^3]\right)^{1/3}}$$

This integral is readily evaluated to obtain

$$(100) \quad \mathcal{I}_2(b) = -\frac{1}{2}\,(\sigma - 1)\left[\left(a_o^3 - (\sigma - 1)^{-1}(b^3 - b_o^3)\right)^{2/3} - a_o^2\right]$$

Note that $\mathcal{I}_2(b)$ can likewise be written in terms of a,

$$(101) \quad \mathcal{I}_2 = -\frac{1}{2}\,(\sigma - 1)\left[a^2 - a_o^2\right]$$

Combining the integrated form for $\mathcal{I}_2(b)$ with Eq. (98) yields the rate law for the time-rate of change of the radius b(t) of the metal

particle. This result also can be obtained by substituting directly Eq. (87) into Eq. (92) and utilizing Eq. (95).

Next let us ask whether or not it is possible to obtain any expressions for the time-dependence of the oxide thickness L and the volume of oxide. Because L=b-a, the above expressions relating b and a to t provide a method to obtain L(t) numerically. More directly, combining Eqs. (84), (85), and (88), the obtained relation

$$(102)\quad V_{oxide} = \sigma\left[\tfrac{4}{3}\pi(a_o^3 - a^3)\right] = \left[\tfrac{4}{3}\pi(b^3 - a^3)\right] - \left[\tfrac{4}{3}\pi(b_o^3 - a_o^3)\right],$$

serves to yield V_{oxide} directly in terms of a and also provides a ready way to obtain L in terms of a. Substituting b=L+a into this relation and solving for L yields

$$(103)\quad L = \left[(1 - \sigma)(a^3 - a_o^3) + b_o^3\right]^{1/3} - a .$$

Numerically the problem can then be evaluated as follows. A sequence of values of a is substituted into Eqs. (92) and (94) to obtain the corresponding sequence of time values. Next the corresponding sequences of values for b, V_{oxide}, and L are obtained from the sequence of values of a by using Eqs. (87), (102), and (103). The results can then be plotted as individual curves, namely, a(t) vs t, b(t) vs t, $V_{oxide}(t)$ vs t, and/or L(t) vs t, as desired.

There will eventually be a point in time where a(t) decreases to zero. Since the metal particle will then have been converted totally to oxide, we designate this as the burn-up time t_{burnup}. The $a(t) \to 0$ limit of Eqs. (92) and (94) yields the time required for the complete oxidation of the spherical particles,

$$(104)\quad t_{burnup} = (\sigma/2\Omega)\left[a_o^2 - \frac{1}{(\sigma - 1)}\left[\left(b_o^3 + (\sigma - 1)a_o^3\right)^{2/3} - b_o^2\right]\right].$$

This can be written in an alternative form involving the quantity b_{max} defined as the value b approaches as $a \to 0$. Then the total quantity of oxide is given by

$$(105)\quad \tfrac{4}{3}\pi b_{max}^3 = \left(\tfrac{4}{3}\pi b_o^3 - \tfrac{4}{3}\pi a_o^3\right) + \sigma\left(\tfrac{4}{3}\pi a_o^3\right)$$

so

$$(106)\quad b_{max} = \left[\sigma a_o^3 + \left(b_o^3 - a_o^3\right)\right]^{1/3} .$$

Thus Eq. (104) can be expressed in the form

$$(107)\quad t_{burnup} = (\sigma/2\Omega)\left[a_o^2 - \frac{1}{(\sigma - 1)}\left(b_{max}^2 - b_o^2\right)\right].$$

Due to the complexity of the above rate laws, little can be deduced from a cursory inspection. Three methods suggest themselves for obtaining physical understanding of the result, *viz.*, numerical evaluations using the scheme outlined above, series expansions, and simplifying approximations. Although we have used all three, at the moment it is most informative to adopt the latter approach. One simplifying assumption which can be made is that the volume expansion

of the oxide is relatively small. In the limit that no expansion of the metal occurs upon formation of the oxide, the volume expansion parameter σ will be unity. The differential equation for a(t) given by Eq. (90) then reduces to

$$(108) \quad -a^2 \frac{da}{dt} \left(\frac{1}{a} - \frac{1}{b_o} \right) = \Omega \ ,$$

since the location of the oxide surface b(t) will then be unchanged with the degree of oxidation, having the initial value b_o . Integration of this expression gives

$$(109) \quad [a_o^2 - a^2] - (2/3b_o)[a_o^3 - a^3] = 2 \Omega t \ .$$

Since $a_o < a$ for spherical particles, and $b_o > 0$, the second bracketed term tends to cancel the first bracketed term on the left-hand side of this equation. Furthermore, the value of the second term will always be smaller than the first term, so that the expression is well-behaved as time increases. The observation to be made is that the time required to reach any given a(t) will be shorter due to the presence of the second bracketed term. As shown later, the first bracketed term expresses the entire planar-limit result for which the radii a and b are much greater that the oxide thickness L=b-a.

The simplified equation above yields the following result for the burn-up time for spherical metal particles,

$$(110) \quad t_{burnup} = a_o^2/6\Omega \ ,$$

where for simplicity we have now assumed there exists no initial oxide (*viz.*, at t=0, $b_o = a_o$).

It is interesting to derive the corresponding result for the oxide thickness L(t) as a function of the oxidation time t. Again assuming σ = 1, we have

$$(111) \quad b = b_o = a + L \ ,$$

so that

$$(112) \quad da = -dL \ .$$

Equation (108) takes the form

$$(113) \quad [1 - (L/b_o)] \ L \ dL = \Omega \ dt \ ,$$

which is readily integrated to obtain the oxide growth rate law for the oxidation of spherical particles,

$$(114) \quad \frac{1}{2} \left(L^2 - L_o^2 \right) - \frac{1}{3b_o} \left(L^3 - L_o^3 \right) = \Omega \ t \ .$$

Often it can be assumed that $L_o = 0$. The cubic term is L is always smaller than the quadratic term, since $L < b_o$, so this equation represents a well-behaved rate law. Furthermore, the cubic term

subtracts from the quadratic term, so a shorter time t is required to reach a given oxide thickness L because of the presence of the cubic term.

It is interesting to compare this result with the corresponding result for planar geometry. The planar limit is achieved by assuming that $L \ll b_o$, so that (L/b_o) can be neglected relative to unity. The differential equation for growth [Eq. (113)] then reduces to the approximate form

$$L\, dL = \Omega\, dt \ , \tag{115}$$

which is integrated readily to yield the planar growth law,

$$L^2 - L_o^2 = 2\, \Omega\, t \ . \tag{116}$$

Comparison of this planar result with Eq. (114) for spherical samples shows that the cubic term contains all of the effects of the spherical geometry.

If a metal plate having an initial thickness $2a_o$ is attacked by oxygen from both sides, then a comparison between the planar result and Eq. (114) above for spherical samples shows that the burn-up time for bare spherical particles of initial radius a_o is only 1/3 the burn-up time required for the plate. Moreover, if the plate is attacked on only one side, the time required for the oxide to reach a thickness on the plate which is equal to the spherical particle diameter would be a factor of 12 larger than the burn-up time of the spherical particle. This simplified example thus serves to illustrate that geometrical effects on the rate of metal oxidation can be quite pronounced.

A numerical computation has been carried out to illustrate the functional form of the simplified rate law [Eq. (114)]. The numerical values used for the several parameters are listed in Table 1. The results of the computation for oxide film thickness L vs time t are shown in Fig. 1. For comparison, the planar result given by Eq. (116) is also plotted in Fig. 1. The faster burn-up of the spherical particles relative to the planar sample as the oxide thickness approaches the value of the initial radius a_o of the metal particle is to be noted in the figure, corresponding to the factor of 3 deduced analytically above. In addition, the rapid increase in the rate as the oxide thickness approaches the value of the initial radius a_o of the metal particle, corresponding to the burn-up point where the radius of the spherical metal particle approaches zero, is of major significance.

References

1. Lynn O. Wilson and R. B. Marcus, "Oxidation of Curved Silicon Surfaces", J. Electrochem. Soc. 134, 481-490 (1987).

2. A. T. Fromhold, Jr., Theory of Metal Oxidation. Vol. I -- Fundamentals (North Holland Publishing Company, Amsterdam, 1976), ch. 7.

3. A. T. Fromhold, Jr., Theory of Metal Oxidation. Vol. II -- Space Charge (North Holland Publishing Company, Amsterdam, 1980), ch. 13.

TABLE 1 -- Values used for the parameters in computing Fig. 1.

$\mu_1 = -1 \times 10^{-8}$ $cm^2/V\text{-}sec$

$\mu_2 = 1 \times 10^{-6}$ $cm^2/V\text{-}sec$

$C_1(a) = 1 \times 10^{14}$ $/cm^3$

$C_1(b) = 5 \times 10^{17}$ $/cm^3$

$C_2(a) = 1 \times 10^{17}$ $/cm^3$

$C_2(b) = 5 \times 10^{17}$ $/cm^3$

$R_1 = -2.0 \times 10^{-22}$ cm^3

$T = 900$ K

$Z_1 = -1$

$Z_2 = 1$

$a_o = 1 \times 10^{-4}$ cm =10,000 Å

$b_o = 1 \times 10^{-4}$ cm =10,000 Å

$\sigma = 1$

$k_B = 1.3806 \times 10^{-23}$ J/K

$e = 1.6022 \times 10^{-19}$ C

Computed Results:

$V_{built\text{-}in} = -0.1210$ Volts

Fig. 1. Oxidation rate law for spherical particles (upper curve) with growth by anion interstitial or cation vacancy diffusion coupled with electron-hole diffusion. The corresponding parabolic law [$L^2 \propto t$] for planar samples (lower curve) is shown for comparison.

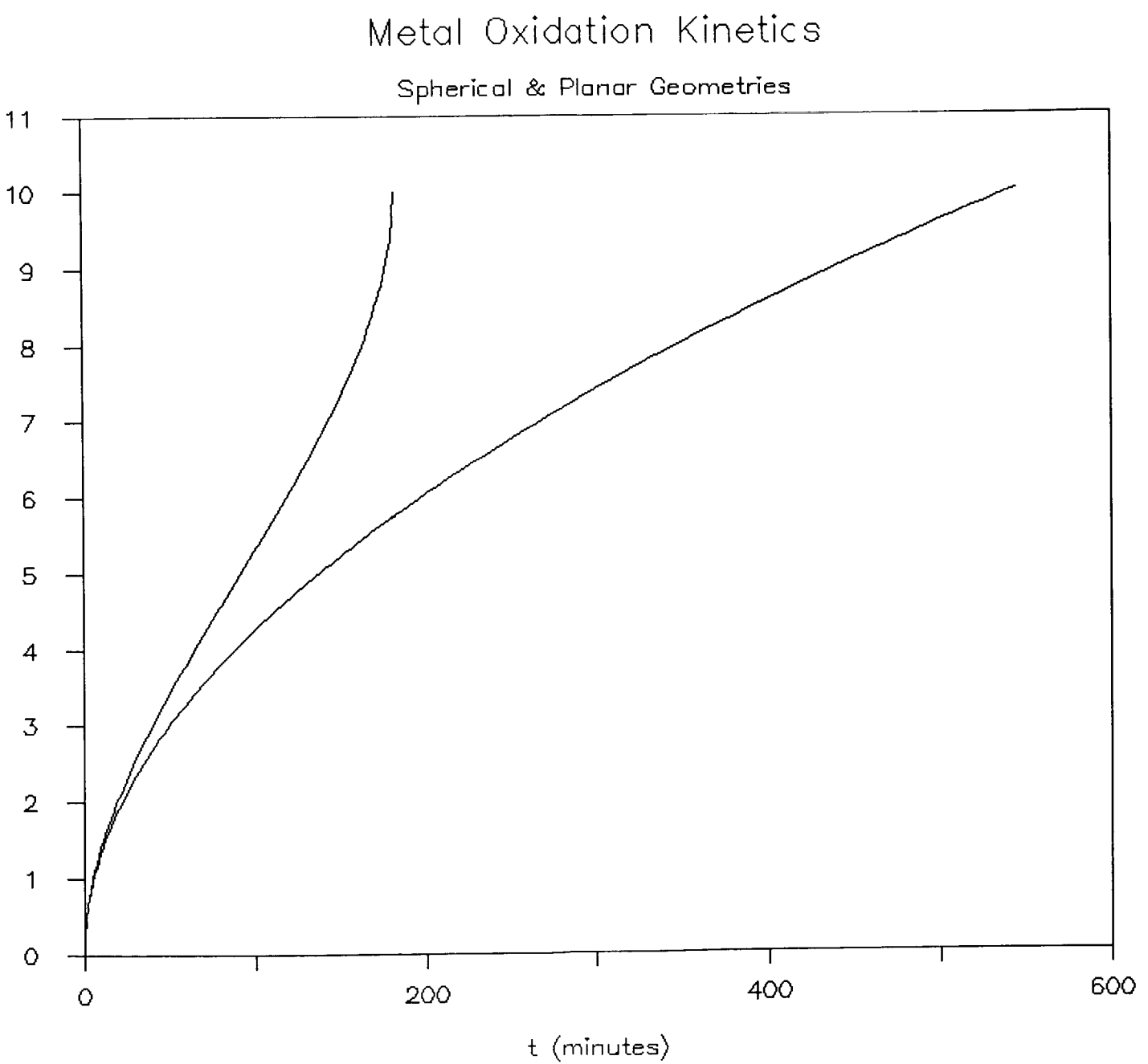
Metal Oxidation Kinetics
Spherical & Planar Geometries
L (angstroms)
(Thousands)
11
10
9
8
7
6
5
4
3
2
1
0
0
200
400
600
t (minutes)